Monthly Notices
of the
ROYAL ASTRONOMICAL SOCIETY

MNRAS **428,** 2824–2839 (2013) doi:10.1093/mnras/sts208

An extensive search for rapid optical variability in ultracool dwarfs

C. Koen★

Department of Statistics, University of the Western Cape, Private Bag X17, Bellville 7535, South Africa

Accepted 2012 October 12. Received 2012 September 25; in original form 2012 June 4

ABSTRACT

In this paper, a summary of optical time-series photometry of 125 ultracool dwarfs is given. The observing strategy was to monitor each object continuously for 2–3 h in order to ascertain whether it was rapidly variable. Many of the targets were observed at multiple epochs, to follow up possible short time-scale variability, or to test for slow brightness changes on longer time-scales. The 353 data sets obtained contain nearly 22 000 individual measurements. Optical (I_C) magnitudes, accurate to roughly 0.1–0.2 mag, were derived for 21 objects for which there is no optical photometry in the literature. It is shown that photometry is affected by variable seeing in a large percentage of the time-series observations. Since this could give the appearance of variability intrinsic to the objects, magnitudes are modelled as functions of both time and seeing. Several ultracool dwarfs which had not been monitored before are variable, according to certain model-fitting criteria. A number of objects with multi-epoch observations appear to be variable on longer time-scales. Since testing for variability is far from being straightforward, the time-series data are made available so that interested readers can perform their own analyses.

Key words: techniques: photometric – brown dwarfs – stars: low-mass.

1 INTRODUCTION

The term 'ultracool dwarf' (UCD) refers here, as is usual, to objects (stars and brown dwarfs) of spectral types late M, L and T. The observational programme reported was primarily concerned with UCDs of spectral class L (106 objects). The modest size of the telescope used (1.9 m) precluded the study of all but three T dwarfs, while only 16 late M dwarfs were included, as the variability properties of these objects are generally much better known.

Since the constituents, and presumably also the structures, of UCD atmospheres are considerably more complex than those of hotter stars, modelling is challenging. The contribution from variability studies is that these could, in principle, shed light on the nature of the atmospheres (as discussed in e.g. Gelino et al. 2002; Goldman 2005). The review by Goldman (2005) lists three mechanisms which could produce flux changes in UCDs: (i) non-homogeneity in the dusty cloud cover at the top of the UCD atmosphere, combined with rotation of the object; (ii) dark, magnetically induced spots, again combined with rotation; and (iii) effects due to close binarity. Mechanism (ii) has been considered unlikely, due to the weak coupling between the atmosphere (which should be largely electrically neutral) and any magnetic effect (see e.g. Meyer & Meyer-Hofmeister 1999; Gelino et al. 2002; Reiners 2012). [Note though the discovery of wide-band optical flares in objects with spectral types as late as M9 (Rockenfeller et al. 2006); distinctly non-thermal radio emission from a number of UCDs (e.g. Antonova et al. 2007); and the detection of variable Hα emission in objects with spectral types as late as L5 (Schmidt et al. 2007)]. The possibility of pulsation could be added to these potential sources of variability (Palla & Baraffe 2005; Cody 2007).

Numerous references to variability studies of UCDs are given in Section 7, where previous work on the targets discussed in this paper is reviewed. Other papers on the flux changes in L and T dwarfs include Martín, Zapatero Osorio & Lehto (2001), Burgasser et al. (2002), Clarke, Tinney & Covey (2002a), Clarke, Tinney & Hodgkin (2003), Artigau, Nadeau & Doyon (2003), Caballero, Béjar & Rebolo (2003), Koen (2006), Artigau et al. (2009) and Radigan et al. (2012). These papers cover observations at wavelengths ranging from the radio, through the near-infrared (NIR) and optical, to X-rays. Of the 125 objects discussed in this paper, 44 had been monitored for variability before; for the remaining 81 stars, time-series photometry is presented here for the first time.

Some previously published photometry by the author (Koen 2003, 2004, 2005) is again included in this paper. The main motivation is that the influence of seeing on the measured differential magnitudes, as discussed in Koen (2009) and Section 5 below, was not taken into account in the original work. In some cases, additional measurements of objects were also obtained subsequent to the initial publications.

The next three sections describe the experimental set-up, give some basic information about the target UCDs (such as magnitudes) and explain the form in which the time-series photometry is made available. The latter is an important part of this paper:

★ E-mail: ckoen@uwc.ac.za

although a number of quantitative measures of variability of UCDs have been proposed (see Koen, Matsunaga & Menzies 2004 for a review), none of these is entirely satisfactory. A contributing factor is the ubiquitous small amplitude trends seen in time-series CCD photometry. This issue has been discussed in a general context by Kovács, Bakos & Noyes (2005), who also developed methodology for correcting the photometry. However, their technique hinges on the availability of a large ensemble of stars in the field of view, whereas fields in the project reported here were generally quite sparse, with as few as a single comparison star.

The main results of this paper are summarized in Table 2, which is discussed in broad terms in Section 6. Aside from the literature reviews, Section 7 also describes the new results for previously studied UCDs. Results for individual objects, which had not previously been monitored for variability, are summarized in Section 8.

Official object names of the targets are listed in Table 1. Since these are rather long, nine-character abbreviations are used elsewhere, made up of the first four digits of the right ascension (RA), sign of the declination and the first four digits of the declination.

Table 1. The observing log, and details of the objects observed. In order, the columns give the object names NIR J magnitude (Skrutskie et al. 2006), I (and, if available, R) magnitudes, information on multiplicity and variability status. If a UCD is a binary, the angular separation between the components (in milliarcseconds) is given in column 5. Otherwise, the following codes are used: X – no information about multiplicity is available in the literature; 0 – the UCD has been checked for multiplicity, with a null result; ? – the object is known to be multiple, but the separation between components is unknown. References for the optical photometry and multiplicity data are numbered in parentheses, and the sources are given at the end of the table. The variability code (column 'Var.') is in two parts: the first summarizes results from the literature (X – no variability information; V – previously detected as variable; C – no variability detected in previous monitoring); a second entry gives the result from this paper (V – variable; C – constant); the third entry, if present (a *Z*), indicates change in nightly mean magnitude (i.e. longer time-scale variability). The last part of the variability entry summarizes the significance level of the estimated seeing function f_s in model (2) [(number of times a significance $\leq$1 per cent is achieved)/ (total number of runs)].

Name	Type	J	I, R [a]	Multiplicity[b]	Var.
2MASS J00145575−4844171	L2.5	14.05	17.54 (1)	X	XC 1/2
2MASS J00361617+1821104	L3.5	12.47	16.05, 18.45 (2); 16.11, 18.35 (7)	90 (8)	VVZ 1/3
2MASS J00464841+0715177	M9	13.89	17.33, 20.23 (8); 17.3 (11)	0 (8)	XC 1/1
2MASS J00584253−0651239	L0	14.31	17.7 (11)	X	CC 0/1
SSSPM J0123−4240	L2.5	13.15	16.28, 19.41 (3)	0 (5)	XC 0/2
2MASS J01282664−5545343	L1	13.78	17.07 (1)	X	XC 1/4
2MASS J01443536−0716142	L5	14.19	17.63 (9)	0 (7)	VV 0/3
DENIS-P J0205.4−1159	L5+L6	14.59	18.44, 20.98 (7); 18.48, 20.61 (8)	390 (1)	CC 0/1
2MASS J02271036−1624479	L1	13.57	16.85 (1)	0 (7)	XC 0/2
2MASS J02284355−6325052	L0.5	13.56	16.71 (1); 16.72, 20.12 (3)	X	XV 0/1
2MASS J02511490−0352459	L3	13.06	16.48 (1); 16.51, 18.85 (2) 16.50, 18.81 (8)	0 (7),(8),(9)	XC 0/1
DENIS-P J0255−4700	L8	13.25	17.21 (1); 17.24, 20.06 (2)	0 (9)	VVZ 3/12
2MASS J02572581−3105523	L8	14.67	17.88 (9)	X	XC 0/2
2MASS J03140344+1603056	L0	12.53	15.8 (11)	0 (5),(8)	XC 0/1
2MASS J03202839−0446358	L0.5	13.26	15.94 (9)	17 (7)	CC 2/2
LP 412-31	M8	12.00	14.64, 17.28 (8); 15.0 (11)	0 (12)	VC 0/2
2MASS J03552337+1133437	L5	14.05	18.08, 20.88 (8); 18.5 (11)	83 (8)	XC 0/1
DENIS-P J035726.9−441730	L0	14.37	17.86 (1)	98 (1)	XC 0/2
2MASS J04082905−1450334	L4.5	14.22	17.55 (1)	X	XC 0/2
SDSS 042348.57−041403.5	L7.5	14.47	18.73, 21.78 (8)	164 (4)	VC 0/1
2MASS J04285096−2253227	L0.5	13.51	16.80 (1)	X	XC 1/2
2MASS J04390101−2353083	L6.5	14.41	17.7 (11)	0 (5)	CC 0/1
2MASS J04455387−3048204	L2	13.39	16.79 (1)	0 (5)	CC 0/3
2MASS J04510093−3402150	L0.5	13.54	16.87 (1)	X	VC 3/4
2MASS J04532647−1751543	L3	15.14	–	X	XC 0/1
2MASS J05002100+0330501	L4	13.67	17.7 (11)	0 (5),(7),(8)	XC 0/1
2MASS J05233822−1403022	L2.5	13.08	16.58 (1)	0 (5),(7)	VCZ 0/4
2MASS J05264348−4455455	M9.5	14.08	17.60 (1); 17.53, 20.00 (2)	X	XC 0/1
SDSS 053951.99−005902.0	L5	14.03	17.99 (1)	0 (1),(7)	VC 1/3
2MASS J05591914−1404488	T4.5	13.80	18.01 (9)	0 (10)	VCZ 1/6
2MASS J06244595−4521548	L5	14.48	18.32 (1)	0 (5)	XC 0/1
2MASS J06411840−4322329	L1.5	13.75	16.97 (1)	X	XCZ 0/2
DENIS-P J0652197−253450	L0	12.76	15.96 (1)	0 (5)	XC 2/2
DENIS-P J0716478−063037	L1	13.90	17.46 (1)	X	XV 2/2
2MASS J07193188−5051410	L0	14.09	17.35 (1)	X	XC 3/5
2MASS J07464256+2000321	L0+L1.5	11.76	15.03, 17.40 (2) 15.11, 17.40 (7); 15.00, 17.77 (8)	219 (1)	VVZ 12/18
DENIS-P J0751164−253043	L1.5	13.16	16.53 (1)	X	XVZ 3/4
DENIS-P J0812316−244442	L1.5	13.82	17.27 (4)	X	XC 2/2

Table 1 – *continued*

Name	Type	J	I, R [a]	Multiplicity[b]	Var.
DENIS-P J0823031−491201	L1.5	13.55	17.14 (1)	X	XC 1/1
SSSPM 0828−1309	L2	12.80	16.07 (1)	0 (7)	VVZ 10/27
2MASS J08290664+1456225	L2	14.75	18.06, 20.56 (8); 18.2 (11)	X	XC 0/1
2MASS J08320451−0128360	L1.5	14.13	17.46 (1); 17.40, 20.03 (8)	0 (1)	XC 0/1
2MASS J08354256−0819237	L5	13.17	17.04 (1)	0 (2),(5),(7)	VV 1/4
2MASS J08355829+0548308	L3	14.53	17.94, 20.69 (8); 17.6 (11)	X	XC 0/2
2MASS J08472872−1532372	L2	13.51	16.84 (1)	0 (5),(7)	CV 1/3
DENIS-P J0909.9−0658	L0	13.89	17.22 (1)	0 (1)	CC 1/3
2MASS J09211410−2104446	L2	12.78	16.50 (1)	0 (4),(7)	XV 4/8
2MASS J09352803−2934596	L0	14.04	17.54 (1)	X	XC 2/2
2MASS J10185879−2909535	L1	14.21	17.42 (1)	X	XC 2/3
2MASS J10452400−0149576	L1	13.16	16.75 (1); 16.51, 18.80 (2) 16.46, 19.15 (8)	0 (5),(7)	CC 1/2
DENIS-P J1047−1815	L2.5	14.20	17.09 (9)	0 (1)	XCZ 0/5
DENIS-P J1048278−525418	L1.5	14.02	17.25 (1)	X	XC 1/1
SDSS 104842.84+011158.5	L1	12.92	16.19, 18.90 (8) α (1)	0 (5),(7)	VV 3/13
DENIS-P J1058.7−1548	L3	14.16	17.73, 20.02 (2); 17.80, 20.10 (7)	0 (2),(9)	XC 1/1
2MASS J11013205−7718249	M8	14.63	17.79 (6); 17.9 (11)	X	VC 0/1
2MASS J11263991−5003550	L9	14.00	17.80 (1)	X	XC 0/1
2MASS J11395113−3159214	M9:	12.69	15.83 (1)	0 (11)	CC 0/6
2MASS J11465791−3914144	M8	13.64	16.47 (1); 16.91, 19.79 (3)	X	XC 1/2
2MASS J11544223−3400390	L0	14.20	17.90 (1)	0 (1)	XC 0/2
DENIS-P J1157480−484442	L0.5	14.01	17.25 (1)	X	XC 0/1
DENIS-P J115927.4−5247188	M9	11.43	14.49 (1)	X	VVZ 4/10
DENIS-P J1159.6+0057	L0	14.08	17.4 (1)	X	XC 0/1
2MASS J12073804−3909050	L4	14.69	17.63 (9)	X	XC 0/3
DENIS-P J1228.2−1547	L5	14.38	17.89 (1); 18.04, 20.41 (2) 18.22, 20.48 (7)	255 (1)	CCZ 2/2
2MASS J12321827−0951502	L0	13.73	16.97 (1)	X	XVZ 2/3
DENIS-P J1253108−570924	L0.5	13.45	16.74 (1)	X	XC 0/1
2MASS J13004255+1912354	L1	12.72	16.00, 18.82 (8); 16.0 (11)	0 (7),(9) 05	VC 1/4
2MASS J13153094−2649513	L5.5	15.20	18.56 (9)	338 (14)	VC 0/1
2MASS J13411160−3052505	L3	14.61	17.75 (9)	X	XCZ 1/2
2MASS J13595510−4034582	L1	13.65	16.99 (1)	X	XC 0/2
2MASS J14090310−3357565	L2	14.25	17.48 (1)	X	VV 1/4
2MASSW 1420544−361322	M7	11.48	14.06 (1)	X	VC 0/1
2MASS J14392836+1929149	L1	12.76	16.12, 18.52 (7) 16.05, 18.81 (8); 16.0 (11)	0 (1),(7),(9)	VC 0/1
DENIS-P J1441−0945	L0.5	14.02	17.41 (1)	373 (1)	VV 1/2
2MASS J15074769−1627386	L5.5	12.83	16.69 (1); 16.51, 18.92 (2) 16.65, 19.04 (7)	? (7)	CC 1/2
DENIS-P J151901.6−741613	M9	13.43	16.56 (1)	X	XC 1/1
2MASS J15200224−4422419	L4.5	13.23	16.89, 19.42 (3)	1174 (6)	XC 2/2
2MASS J15230657−2347526	L2.5	14.20	17.33, 20.42 (3)	X	XC 0/3
2MASS J15344984−2952274	T5+T5	14.90	19.4 (11)	65 (10)	VCZ 0/3
DENIS-P J153941.96−052042.4	L3.5	13.92	17.47 (1)	0 (2),(5),(7)	XCZ 0/8
2MASS J15474719−2423493	L0	13.97	17.16 (1)	X	XC 0/3
2MASS J15485834−1636018	L2	13.89	17.04, 19.93 (3)	X	XC 0/1
2MASS J15551573−0956055	L1	12.56	15.74 (1)	0 (7)	VC 1/3
SDSS 155526.15+001720.6	L0	14.95	18.19 (1); 17.98, 21.09 (8)	X	XC 1/1
LSR J1610−0040	sdM7	12.91	14.81, 17.51 (5) 15.02, 17.22 (8); 14.80 (9)	31 (16)	XC 1/3
2MASS J16154245+0546400	M9	12.88	16.06, 18.93 (8); 15.9 (11)	X	XC 1/2
2MASS J16184503−1321297	L0	14.25	17.88 (1)	X	XC 1/2
SDSS 161928.3+005011.9	L2	14.39	17.79 (1); 17.89, 20.65 (8)	0 (1)	XC 1/1
2MASS J16304139+0938446	L0	14.87	18.32, 21.05 (8); 18.3 (11)	X	XC 0/1
SDSS 163600.79−003452.6	L0	14.59	17.59 (1); 17.68, 20.42 (8)	X	CC 0/1
2MASS J16452211−1319516	L1.5	12.45	15.68 (1)	0 (7)	CC 0/1
2MASS J16573454+1054233	L2	14.15	17.54, 20.20 (8)	X	XC 1/1
DENIS-P J170548.38−051645.7	L4	13.31	16.55 (1)	0 (2),(5),(7)	VVZ 6/7
DENIS-P J17054744−5441513	M8.5	13.64	16.66 (1)	X	XC 2/2
DENIS-P J1745346−164053	L1.5	13.65	17.11 (1)	X	XC 0/2
2MASS J17502484−0016151	L5.5	13.29	17.33, 19.98 (3); 16.40 (9)	0 (2)	XC 0/1

Table 1 – *continued*

Name	Type	J	I, R [a]	Multiplicity[b]	Var.
2MASS J17534518−6559559	L4	14.10	17.80 (1)	0 (5)	XC 0/2
DENIS-P J1756561−480509	L0	13.41	16.76 (1)	X	XC 1/2
DENIS-P J175629.6−451822	M9	12.39	15.46 (1)	X	XC 0/1
2MASS J18212815+1414010	L4.5	13.43	17.0 (11)	0 (7)	XC 0/3
DENIS-P J1909081−193748	L1	14.52	17.92 (1)	X	XC 0/1
2MASS J19285196−4356256	L4	15.20	18.43 (9)	0 (2)	XCZ 0/2
2MASS J19360187−5502322	L5	14.49	17.9 (11)	0 (5)	XC 1/2
2MASS J19561542−1754252	M8	13.75	16.88, 20.09 (3)	X	XC 2/2
2MASS J20261584−2943124	L1	14.80	18.21 (1)	<250 (15)	XV 0/3
SDSS J202820.32+005226.5	L3	14.30	17.83 (1); 17.80, 20.50 (8)	0 (9)	CC 0/2
2MASS J20343769+0827009	L3	14.46	17.9 (11)	0 (2)	XC 1/3
2MASS J20360316+1051295	L3	13.95	17.4, 20.2 (11)	0 (7),(8)	XC 0/2
2MASS J20414283−3506442	L2	14.89	18.32 (1)	X	XC 1/2
2MASS J20450238−6332066	M9	12.62	16.05 (1)	X	XC 0/1
2MASS J20575409−0252302	L1.5	13.12	16.61 (1)	0 (5),(7)	VV 1/2
2MASS J21041491−1037369	L2.5	13.84	17.2 (11)	0 (2),(5),(7)	VC 2/3
2MASS J21304464−0845205	L1.5	14.14	17.38 (1); 17.35, 19.78 (2)	X	CVZ 2/6
2MASS J21371044+1450475	L2	14.13	17.1 (10); 17.3 (11)	X	XC 0/1
2MASS J21501592−7520367	L1	14.06	17.53 (1)	X	XC 0/1
2MASS J21574904−5534420	L2	14.26	17.36 (1)	X	XC 0/2
2MASS J21580457−1550098	L4	15.04	18.58, 20.77 (2)	0 (1)	CC 0/1
DENIS-P 220002.05−303832.9AB	L0	13.44	16.5 (11)	1090 (13)	XV 1/1
ϵ Indi Bab	T5	11.91	16.63 (9)	732 (11)	VVZ 6/6
2MASS J22244381−0158521	L4.5	14.07	18.02, 20.29 (7); 17.7 (11)	0 (2)	VC 1/4
2MASS J22431696−5932206	L0	14.07	17.27 (1); 17.37, 20.24 (3)	X	XV 0/1
DENIS-P 225210.73−173013.4	L7.5	14.31	17.89 (1)	130 (3)	XC 0/1
SSSPM J2310−1759	L0	14.38	17.42 (1); 17.47, 19.37 (2)	X	XC 1/1
2MASS J23224684−3133231	L0	13.58	16.84 (1)	X	XC 0/1
2MASS J23515044−2537367	M8	12.47	15.41 (1)	0 (5)	XV 2/3

[a]The sources of the optical photometry in the fourth column are (1) The DENIS Third Release Catalogue (Epchtein et al. 1999); (2) Liebert & Gizis (2006); (3) Kendall et al. (2007); (4) Phan-Bao et al. (2008); (5) Burgasser et al. (2007a); (6) Luhman (2007); (7) Dahn et al. (2002); (8) transformed from SDSS i and z photometry; (9) from DENIS photometry of a star in the field of view; (10) from SDSS photometry of a star in the field of view; (11) from zero-point set during the night.

[b]Sources of the multiplicity data are (1) Bouy et al. (2003); (2) Burgasser et al. (2010); (3) Reid et al. (2006a); (4) Burgasser et al. (2005); (5) Reid et al. (2006b); (6) Burgasser et al. (2010); (7) Blake, Charbonneau & White (2010); (8) Bernat et al. (2010); (9) Reid et al. (2008); (10) Burgasser et al. (2003); (11) McCaughrean et al. (2004); (12) Close et al. (2003); (13) Burgasser & McElwain (2006); (14) Burgasser et al. (2011); (15) Gelino & Burgasser (2010); (16) Dahn et al. (2008).

2 THE OBSERVATIONS

All the photometry reported in this paper was obtained with the South African Astronomical Observatory (SAAO) CCD camera mounted on the 1.9-m telescope at Sutherland. The camera is equipped with a 1024 × 1024 chip, giving a field of view of about 2.5 arcmin^2. All observations were pre-binned 2 × 2, resulting in a read-out time of about 20 s. The aim was to spend a minimum of two to three hours observing each target, with exposure times determined by target brightness and weather conditions. Targets which showed signs of variability were observed again, circumstances permitting.

All but two of the 125 targets for which results are presented were observed through a Cousins I filter; of these, 33 were also monitored in R. A few isolated measurements were made through a Z filter or in white light (i.e. with no filter in the light beam). The choice of filters was dictated to some extent by necessity: given the modest telescope aperture, and the relative faintness and extreme red colours of the targets, broad-band filters at the red end of the optical spectrum were the only sensible choices. Wherever practically possible (i.e. for the brighter targets, under good observing conditions), observations were alternated between R and I, since, at least in principle, information about physical conditions could be deduced by comparison of variability patterns in different wavebands (see e.g. Koen 2008). A handful of observations made in Z or white light were largely by way of experiments.

Multiple sets of observations were obtained for 78 of the targets. The mean length of the 353 individual data sets is 3.1 h, and the mean number of measurements per data set is 62.

Photometric reductions, performed with DOPHOT (Schechter, Mateo & Saha 1993), were completely standard. Point spread function (PSF) photometry was used throughout, as it was generally found to be far more accurate for the faint objects measured. All UCD measurements were differentially corrected to remove as far as possible the effects of atmospheric transparency changes.

3 SOME BASIC INFORMATION ABOUT THE TARGET OBJECTS

The first column of Table 1 shows the full 'discovery name' of the UCD, extracted from http://spider.ipac.caltech.edu/staff/davy/ARCHIVE/index.shtml although in the case of Two Micron All Sky Survey (2MASS; Skrutskie et al. 2006) objects, the finally adopted name has been substituted. Spectral

classifications in the second column of the table have been taken from the SIMBAD data base. The use of these resources is gratefully acknowledged.

Given the limitations of the telescope and instrumentation, only relatively bright UCDs were monitored. By implication the objects are nearby, and it is therefore not surprising that many have shown considerable proper motion since their discovery. This was particularly noticeable when searching for more recent Sloan Digital Sky Survey (SDSS; Adelman-McCarthy et al. 2009) photometry of the targets. Some striking examples are LP 412-31 (4 arcsec change in position since discovery), 0355+1133 (5 arcsec), 1300+1912 (9 arcsec) and 1439+1929 (10 arcsec).

For 60 per cent (75 out of 125) of the objects, I magnitudes are listed in the third release of the Deep Near Infrared Survey of the Southern Sky (DENIS) catalogue (Epchtein et al. 1999). 22 objects in Table 1 have SDSS photometry. The equations

$$I = i' - 0.3780(i' - z') - 0.3974,$$
$$R = r' - 0.2936(r' - i') - 0.1439$$

were used to transform the latter to Cousins I and R (http://www.sdss.org/dr6/algorithms/sdssUBVRITransform.html#Lupton2005). There are six objects with both DENIS and SDSS photometry: differences are $I(\mathrm{DENIS}) - I(\mathrm{SDSS}) = -0.10, -0.09, -0.02, 0.03, 0.06$ and 0.21 mag, i.e. the transformation works well.

Liebert & Gizis (2006) list R and I magnitudes for 13 objects. Eight of these are common to the DENIS catalogue: the largest difference in I magnitudes is 0.24 mag, the mean difference being 0.03 mag. Two Liebert & Gizis (2006) objects are also in the SDSS catalogue: the I magnitudes agree to 0.05 mag and the R magnitudes to within 0.4 mag. Kendall et al. (2007) measured R and I (in the SuperCOSMOS system) of nine of the objects in the present sample. Three of these also have DENIS I photometry: differences between the duplicated measurements are $I(\mathrm{DENIS}) - I(\mathrm{SuperCOSMOS}) = -0.01, -0.10$ and -0.44 mag. R and I magnitudes for seven UCDs in Table 1 are available in Dahn et al. (2002). Their photometry agrees very well for the four objects in common with Liebert & Gizis (2006). Agreement with SDSS photometry is also reasonable.

Measurements of single objects have been taken from Burgasser, Cruz & Kirkpatrick (2007a), Luhman (2007) and Phan-Bao et al. (2008).

For 22 objects, no I-band measurements could be found in the literature. For 10 of these 22 objects, DENIS photometry was available for a star in the same SAAO CCD field as the UCD. The mean SAAO I magnitude difference between the UCD and star with known brightness could be used to calculate the magnitude of the former. For a further 11 objects, use was made of stars or UCDs with known magnitudes, which were observed during the same night, to set the photometric zero-points for the night. For a given UCD, magnitudes obtained on different nights by the latter method generally agreed to within 0.1–0.2 mag. The R and I magnitudes of one object were determined from SDSS photometry of a star in the same field.

Given the different filters used, and a lack of proper standardization for objects as extremely red as the UCDs, it seems pointless to belabour differences between different determinations of I. Only a few comparisons are therefore made of magnitudes derived from photometry at SAAO, with previously published values. The SuperCOSMOS magnitude of 1610−0040 is quoted by Burgasser et al. (2007b) as $I = 14.8$, whereas the transformed SDSS magnitude is $I = 15.02$, and the value derived from comparison to a DENIS star in the field is $I = 14.80$. Magnitude differences for 1750−0016, by contrast, are large: SuperCOSMOS $I = 17.22$ (Kendall et al. 2007) while $I = 16.40$ by comparison with a DENIS star in the field of view of the SAAO photometry.

Magnitudes determined by the nightly zero-point method agree remarkably well with transformed SDSS photometry of the stars – the mean difference, over nine objects, is 0.04 mag. The largest discrepancy of 0.4 mag is for the rather faint 0355+1133 ($I > 18$).

Only one UCD, 0453−1751, remains with no I-band magnitude assigned.

The $I - J$ colour index is plotted against I in Fig. 1, which shows that the bulk of the objects have I magnitudes between 15.5 and 18.5. It is noticeable that redder objects are all faint, with the exception of the very nearby ϵ Indi Bab. Fig. 2 presents two-colour diagrams. Values plotted are averages of actual measurements, where available. Indirect determinations were used in cases where no direct measures are available. In view of the difficulty of obtaining precision photometry of UCDs, as referred to above, as well as the uncertainties involved in indirect magnitude determinations, it is not possible to supply reliable error estimates for the plotted points.

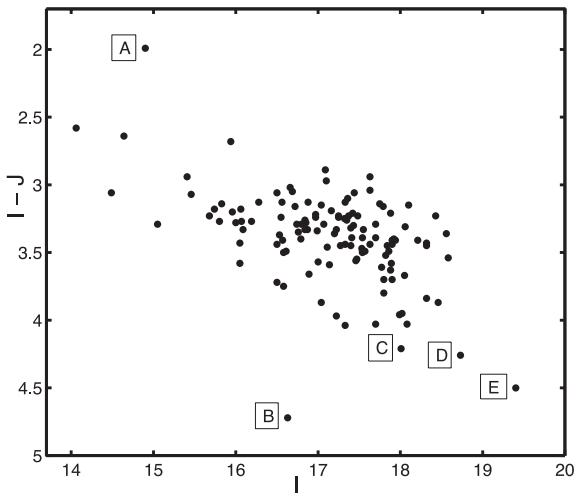

Figure 1. A colour–magnitude plot for 124 of the 125 targets. The outlying points, marked by letters, correspond to objects with extreme spectral types (see the text).

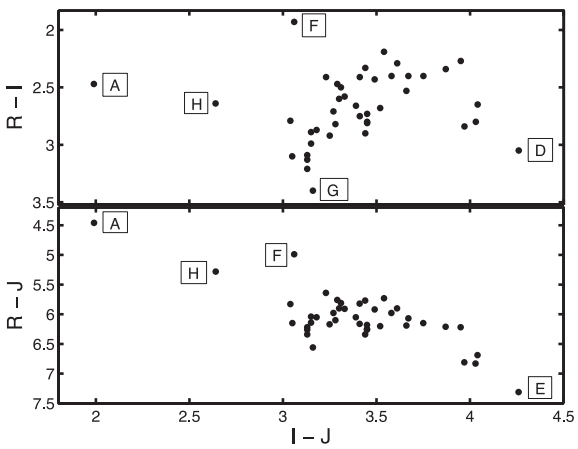

Figure 2. Two-colour diagrams for 42 of the UCDs for which R magnitudes are available. Objects corresponding to the marked outlying points are noted by name in the text.

For some objects multiple measurements are listed in Table 1, and these could be compared in order to gain a rough idea of the photometric errors.

The outlying points are as follows. A: 1610−0040 (sdM7); B: ϵ Indi Bab (T5); C: 0559−1404 (T4.5); D: 0423−0414 (L7.5); E: 1534−3952 (T5+T5); F: 2310−1759 (L0); G: 0228−6325 (L0.5); H: LP 412-31 (M8). The tight group of three points between E and the bulk of the points in the lower panel of Fig. 2 correspond to late L UCDs (spectral types L5–L8).

The only real surprises are 2310−1759 (F) and 0228−6325 (G) which, respectively, seem too bright and too faint in *R*, compared to their *I* and *J* magnitudes. Of course, the first explanation which comes to mind is that the photometric errors in *R* may be very large. Unfortunately, in both cases there is only a single source of *R* photometry.

The penultimate column of Table 1 contains information about multiplicity of the UCDs. This information is particularly pertinent because close doubles are measured as single objects, and, as discussed at length in Section 5 below, this may have unfortunate consequences for the reliability of the PSF photometry.

The last column of the table shows an assessment of variability. As mentioned in Section 1, there is no entirely reliable method that can be used to assess whether an object is constant or not. For this reason the individual data sets are made available, so that interested readers can analyse these, and draw their own conclusions. Column 6 of Table 1 contains the author's assessment of variability, according to the subjective criteria given in Section 6. Codes are explained in the table caption.

4 THE TIME-SERIES DATA

A log of the observations is given in the first seven columns of Table 2.

There is a data file available electronically only for each of the 353 time series of observations. Filenames start with the first four digits of the object's RA, followed by the filter name (*I*, *R*, *Z* or *W* – the last indicating 'white light', i.e. no filter). After the filter name is the sequence number of the observations through the particular filter. As an example, the file '1341I3' contains the third set of *I*-band observations of 2M 1341−3052. In cases where the first four digits of the RA are not unique, the sign and first two digits of the declination are also used, e.g. '1048+01R2' for the second set of *R* filter observations of SDSS 1048+0111.

The first column of each data file contains the fractional part of the Heliocentric Julian Day (HJD), the second column is the estimated seeing (full width at half-maximum in arcseconds) and the third column is the PSF photometry of the UCD. Subsequent columns contain PSF photometry of one or more stars in the field with brightnesses similar to that of the UCD. Plotting the additional photometry along with that of the UCD allows the light curve of the latter to be seen in the proper context. Since the observations were obtained under a variety of atmospheric conditions, the photometry was routinely standardized with respect to a few stars in the field of view, i.e. all observations have been differentially corrected.

There is a single instance, namely the *R* filter observations of 2M 1300+1912, in which the field contained only one object aside from the UCD. Since the former was used for standardization, there are no comparison data for the UCD photometry.

In the vast majority of cases the fields overlapped when UCDs were observed at multiple epochs, hence a given column of photometry will refer to the same comparison object across multiple files. For example, data for the same three comparison stars are given in columns 4–6 of 0746I1–0746I9. It should be noted though that different sets of comparison stars were selected for different filters. The code for a missing observation is −99.0000; single missing values are due to the removal of outlying points (more than 4σ from the mean value). A column of missing values implies that the particular comparison star, although measured at several other epochs, was not in the field of view of the particular run.

A few exceptions are the following: 2351I1 and 2351I2 refer to different fields; 0828I1–0828I14 all refer to the same field, but photometry in 0828I15 is from a different field; 0828R1 and 0828R12 are from distinct fields, while 0828R2–0828R11 all refer to the same field.

A few comparison stars with small scatter in their photometry were used to set zero-points across different nights. Unfortunately, the relative brightnesses of apparently constant stars typically vary by a few per cent from night to night. This is no doubt due to a variety of reasons – slow variability of the stars, small drifts in the photometry due to instrumental effects and the fact that

Table 2. The observing log (columns 2–6), and some quantities derived from the photometry (columns 7–12). Filters '*R*' and '*I*' are Cousins R_C and I_C, while '*W*' indicates white light (i.e. no filter). Entries under '*T*' are run lengths, in hours, and *N* indicates the number of useful exposures obtained. The standard deviation of the measurements is given by σ. Columns 8–11 contain the results of regressing the photometry on seeing (linearly) and time (an unspecified non-parametric fit): β_s is the slope of the seeing regression, and *p*(seeing) its *p*-value; the *p*-value of the regression on time is denoted '*p*(time)', and R^2 is the proportion of variance explained by the fit. Six data sets were too short ($N < 10$) for the fit to be attempted. For the 10 data sets with bright outlying points (see Section 4) a second regression solution, excluding the outlier, was obtained; these results are also provided. The last column is the offset of the night's photometry from the brightest mean over all nights. An 'X' indicates that no value could be calculated (i.e. the particular star/filter combination occurred only once). Further details are given in the text. A full version of this table is available online only.

Name	Start HJD (245 0000+)	Filter	*T* (h)	Exp. time (s)	*N*	σ (mmag)	β_s (mmag arcsec^{-1})	*p*(seeing)	*p*(time)	R^2	Zero-point (mmag)
0014−4844	4322.5061	*I*	3.9	120	100	16	−15.7	0.001	0.001	0.564	0
	5045.6349	*I*	1.4	180	25	8	−14.9	0.602	0.399	−0.011	35
0036+1821	3621.5155	*I*	2.8	120	70	15	−29.4	0.000	0.000	0.621	56
	3622.4136	*I*	4.2	90	38	16	−5.9	0.179	0.000	0.444	0
	3622.4158	*R*	3.6	240	34	7	−4.2	0.506	0.026	0.197	X
0046+0715	5046.5877	*I*	2.3	240	33	6	−18.7	0.005	0.058	0.195	X
0058−0651	3941.5790	*I*	2.6	120	64	13	−14.0	0.060	0.001	0.214	X
0124−4240	4324.5629	*I*	2.6	180	46	5	−5.6	0.163	0.280	0.004	0
	4326.5041	*I*	2.2	120	56	7	0.3	0.942	0.061	0.111	7

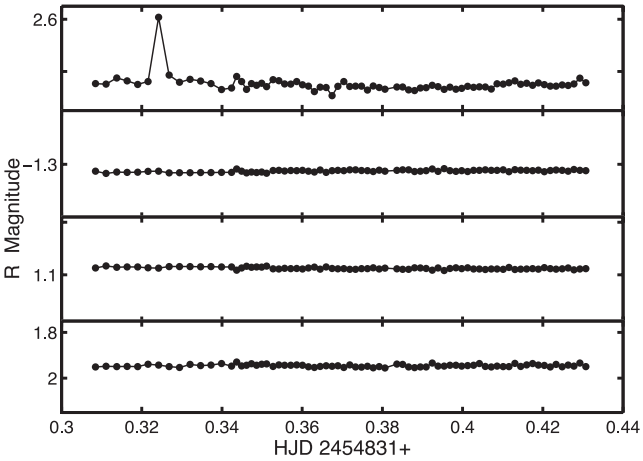

Figure 3. Time-series photometry of LP 412-31, in the *R* band, showing an apparent short-lived flare (top panel). The lower panels give the photometry of three stars in the field of view. The scales on the four axes are the same. The photometric zero-point in the figure is arbitrary, but the true relative brightnesses of the objects are shown.

differential corrections were not always made with respect to the same collection of local standard stars.

Outlying bright points in UCD observations have generally been retained, where 'outlying' is defined as being more than 4σ above the mean level. Although occasional bright outliers were also seen in the comparison star data (and were removed), the likelihood that these may be due to flares is probably lower than in the case of the UCDs. Furthermore, although no formal test was carried out, it certainly appears that a disproportionate number of bright outliers were found in the UCD data. Data sets with single bright points are 0255R1 (36), 0320+18R1 (7), 1047I3 (20), 1409I2 (40), 1539R1 (45), 1645I1 (78), 2104I3 (70) and 2224I3 (14), where numbers in brackets are sequence numbers of the outliers. Two sets of observations of DENIS 1705−0516 showed bright outliers: 1705−05I2 (12) and 1705−05I4 (77 and 120) – but note the bright outliers (albeit more moderate) in the accompanying comparison star data.

An important point is that there are *no* instances of a succession of bright outliers, as would have be expected if there were extended flares. In other words, as far as the *I* and *R* filters are concerned, flares are either insignificant in amplitude and/or duration.

Some examples of the data are shown in Figs 3–6. In order, these plots demonstrate a possible short-lived flare in LP 412-31, likely short-time-scale variability in 0921−2104, similar time trends in the photometry of 1228−1547 and variability on a time-scale of days in the brightness of 0559−1404.

5 THE INFLUENCE OF SEEING ON MEASURED MAGNITUDES

Since the amplitudes of brightness changes in UCDs are small, it is important to account for sources of variability which may not be intrinsic to the objects themselves. Koen (2009) pointed out that stellar magnitudes determined by the fitting of PSFs may be affected by seeing. He demonstrated the effect by fitting time series of observations by a sum of two functions, one describing time dependence and the other seeing dependence of measured magnitudes. It was found that the seeing dependence, when present, is often roughly linear, with objects measured brighter when the seeing is larger.

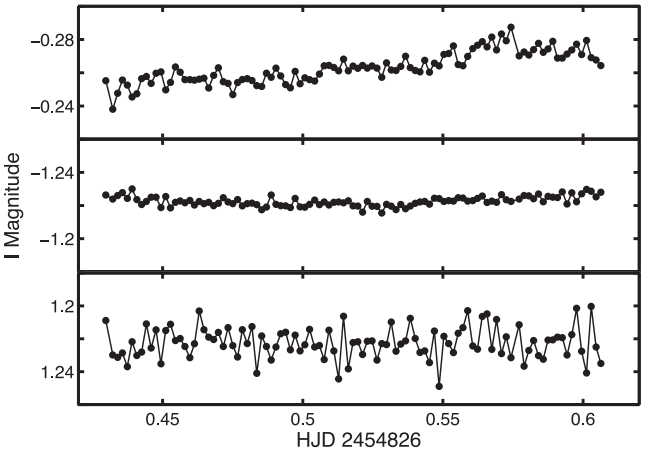

Figure 4. Same as Fig. 3, but showing *I*-band photometry of 0921−2104 and two comparison stars. The UCD appears to be variable.

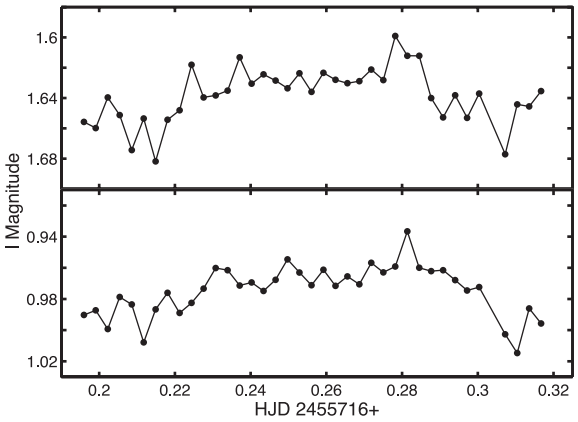

Figure 5. Same as Fig. 3, but showing *I*-band photometry of 1228−1547 and a comparison star. Similar trends can be seen in both light curves.

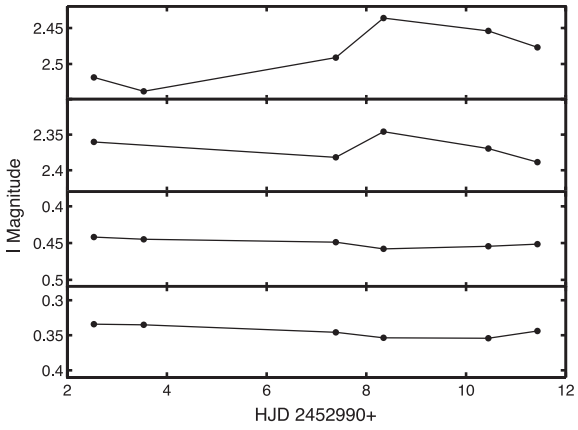

Figure 6. The mean *I* magnitude of 0559−1404 over the six nights during which it was observed (top panel). The other panels show the mean magnitudes of three stars in the field of view.

Figs 7–9 illustrate the effect. The first of these plots shows time-series photometry of 2200−3038 (middle light curve) which clearly seems to vary somewhat irregularly. Fig. 8 demonstrates that while the comparison star data are independent of seeing, there is an almost-linear relationship between brightness and seeing for 2200−3038. A straight line was therefore fitted to these data:

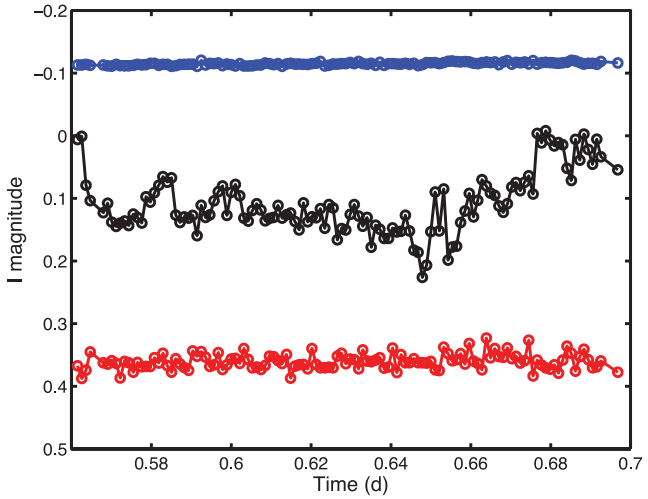

Figure 7. Time-series photometry of 2200−3038, obtained on JD 245 3172 (middle light curve). For comparison, light curves of two stars in the field are also plotted (data set 2200I1). Photometric zero-points for the three light curves are arbitrary (the true mean magnitude of the top plot data is roughly 1.1 mag brighter than the 2200−3038 data, and the mean magnitude of the bottom plot data is about 1 mag fainter than 2200−3038.

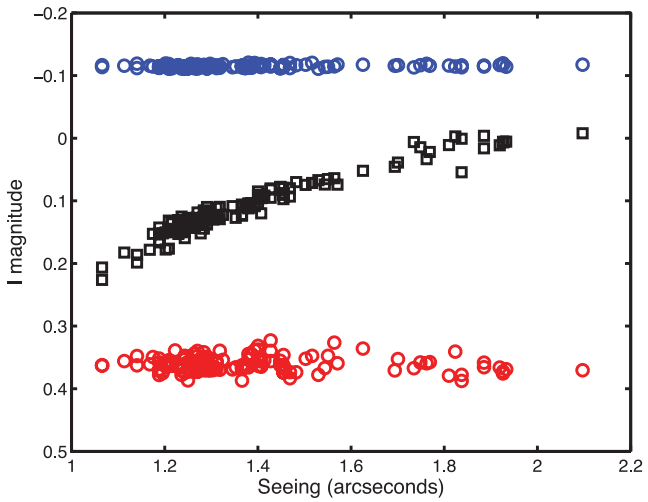

Figure 8. Same as Fig. 7, but with PSF magnitudes plotted against seeing rather than time.

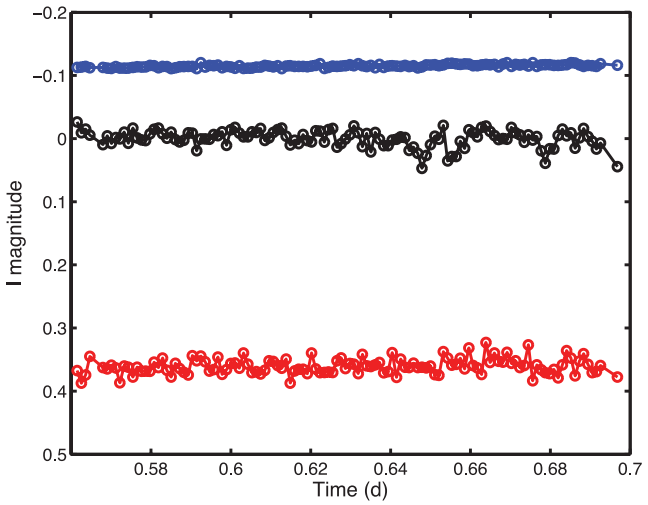

Figure 9. Same as Fig. 7, but the photometry of 2200−3038 has been pre-whitened by a linear fit to its seeing dependence (see the text for details).

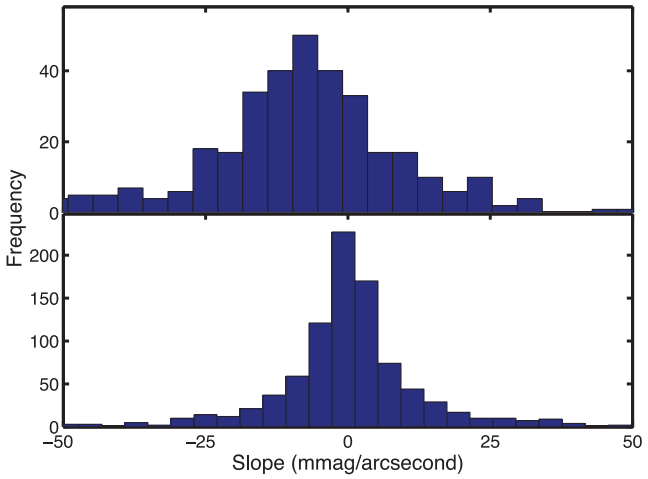

Figure 10. The results of linear regression of magnitudes on seeing for the UCDs (top panel) and comparison stars (bottom panel). Shown are the frequency distributions of the slopes (measured in mmag arcsec^{-1}). For the UCD data, 7.1 per cent of the values are outside the range of the plot; for the comparison data the figure is 2.6 per cent.

subtracting the fit, and plotting the residuals against time (Fig. 9) leads one to believe that the apparent variability in Fig. 7 is spurious.

Koen (2009) speculated that the underlying cause of the seeing dependence of PSF magnitudes may be multiplicity of the objects: if component separations are only slightly below the best resolution limit, then seeing will strongly affect the observed PSF, and hence the measured brightness of the object. If this is correct, and if multiplicity amongst UCDs is common (Jao et al. 2009 put it at ∼26 per cent), it may be expected that the effect will be much more prevalent in small-telescope photometry of UCDs than of stars. This follows since only nearby objects are bright enough to be observable – hence angular separations between UCD components will generally be substantially larger than with binary stars of similar brightness.

The point is explored by Figs 10 and 11 (see the online version of this paper for the latter figure). The information plotted is based on linearly regressing PSF magnitudes on seeing, both for the UCDs (353 data sets), and for the comparison star observations (914 data sets) in the data files. The bottom histogram in Fig. 10 shows that positive and negative regression slopes are roughly equally likely for the comparison star data, whereas there is a distinct preference for negative slopes in the case of the UCDs. The comparison slopes are also much more concentrated around zero than the UCD slopes. Fig. 11 presents a different view: actual slopes are plotted on the horizontal axis, while the vertical axes show the 'standardized' absolute values of the slopes (i.e. a rough measure of significance). The excess of highly significant negative slopes is particularly noteworthy.

The best one could have hoped for is a clear separation between objects which show minimal dependence of brightness on seeing, and those for which magnitudes are strongly negatively correlated with seeing. Unfortunately this is not always the case, as illustrated by observations of 1048+0111 plotted in Figs 12 (time dependence) and 13 (seeing dependence). Fitting straight lines to the data in

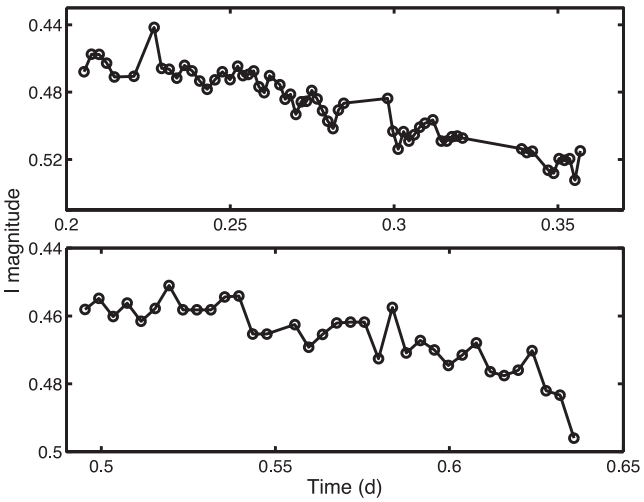

Figure 12. The results of two photometric runs on 1048+0111, on JD 245 2770 (1048+01I3 – top panel) and JD 245 3411 (1048+01I4 – bottom panel).

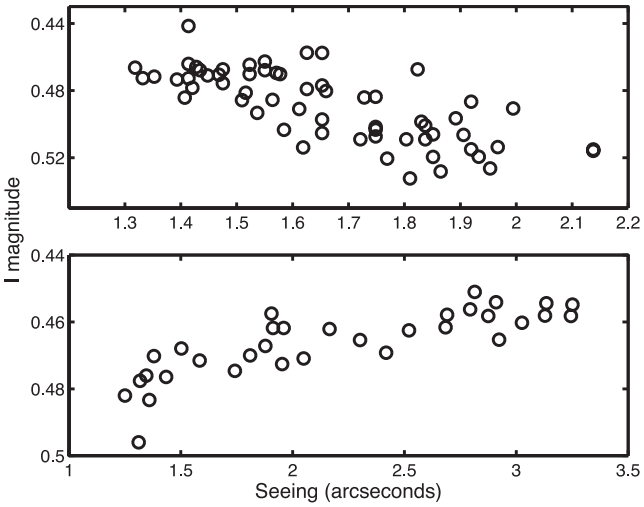

Figure 13. Same as Fig. 12, but with PSF magnitudes plotted against seeing rather than time.

Fig. 13 gives slopes standardized by their standard errors of −7.8 and +8.3, respectively, both highly significant – as could have been anticipated from the figure. The large positive slope is unexpected in view of the results above, and also because it may be expected that, for a given object, the dependence of the measured magnitude on seeing should always be the same. The likely explanation is that the object is intrinsically variable, and that measured brightnesses may depend on both time and seeing. It is therefore necessary to regress magnitudes simultaneously on both these independent variables.

Koen (2009) describes the application of a non-parametric multivariate regression technique, 'Generalized Additive Model' (GAM) fitting, to this problem; see Hastie & Tibshirani (1990) and Wood (2006) for extensive treatments. The basic idea is to describe the measurements m by the model

$$m(t, s) = \alpha + f_{\rm s}(s) + f_{\rm t}(t) + e(s, t), \quad (1)$$

where t and s are time and seeing, α is a constant, $f_{\rm s}$ and $f_{\rm t}$ are smoothly varying functions of seeing and time, respectively, and $e(s, t)$ are the regression residuals. The precise forms of the functions $f_{\rm s}$ and $f_{\rm t}$ are left unspecified: these are determined by the data, as in non-parametric data smoothing methods.

Time sampling is generally regular (exposures were obtained at fixed intervals), but seeing sometimes varied erratically. This causes a problem, in that there may be outlying seeing values which would exert undue influence on the derived form of $f_{\rm s}$ in equation (1). Since experience shows that the dependence of magnitude on seeing is generally close to linear, the problem can be circumvented by specifying a parametric – linear – form for $f_{\rm s}$:

$$m(t, s) = \alpha + \beta_{\rm s} s + f_{\rm t}(t) + e(s, t)\,. \quad (2)$$

Equation (2) was fitted to all data sets with a reasonable number of observation ($N \geq 10$), using the R software package MGCV (Wood 2006). Reasons for this choice of GAM implementation are discussed in Koen, Kanbur & Ngeow (2007). The results are reported in columns 8–11 of Table 2. Columns 8 and 9 contain values of $\beta_{\rm s}$ and its significance level. (The latter is specified in terms of the 'p-value', i.e. the probability of observing a slope of that magnitude by chance.) Column 10 shows the p-value associated with $f_{\rm t}$, and column 11 gives a standard regression statistic R^2, the fraction of the data variability described by the model.

Two points need to be made. The first is that in cases where $\beta_{\rm s}$ were not significant (at the 5 per cent level),

$$m(t) = \alpha + f_{\rm t}(t) + e(t) \quad (3)$$

was fitted to the data, since it was deemed that seeing plays no role in determining magnitudes. In such cases, columns 8 and 9 report the fitting of equation (2), while columns 9 and 10 give the results of fitting equation (3).

The second point concerns the appearance of a few negative values of R^2 in Table 2. This happens in cases where the fitted model is inferior to simply using the series mean as a model for the data.

Of the 347 slopes $\beta_{\rm s}$ in Table 2, only 91 (i.e. 26 per cent) are positive, and only 23 (15) of these are significant at the 5 per cent (1 per cent) level. By contrast, 128 (96) of the negative slopes are significant at the 5 per cent (1 per cent) level. It is noteworthy that in a list of UCDs with multiple runs and highly significant positive $\beta_{\rm s}$ ($p < 0.01$), all but two have multiple occurrences. This suggests that very large positive slopes may be due to real effects, rather than be statistical aberrations.

6 VARIABILITY REVEALED BY THE INFORMATION IN TABLE 2

In this section, an attempt is made to draw general conclusions (although some specific results will be highlighted). Detailed discussion of individual objects will be combined with the literature review of the next section (for previously studied objects) or will be dealt with in Section 8 (in the case of newly monitored UCDs).

6.1 Standard deviations

The distribution of standard deviations of the data sets is plotted in the top panel of Fig. 14 (online only). This may be compared to the corresponding histogram for the comparison star data in the bottom panel of the figure. There is clearly a tendency towards larger values amongst the UCD data, but probably not to the extent that this can be used as a means of identifying clear-cut variability. Only 11 UCD data sets have $\sigma \geq 35$ mmag, and these are discussed next.

The three largest values of σ have not been included in the histogram for the UCD data in order to make the plot clearer. By far the largest value is $\sigma = 71$ mmag (1534I4), but this is based on a very small data set – $N = 7$. (Similarly, $N = 8$ for 1341I2, for which $\sigma = 38$ mmag.) For 2200I1, $\sigma = 49$ mmag, and almost all the variability can be explained by seeing variations ($R^2 = 0.93$). Similar considerations apply to 2204I3 ($\sigma = 36$ mmag, $R^2 = 0.93$) and 2130I2 ($\sigma = 35$ mmag, $R^2 = 0.91$). For a number of R-band data sets the standard deviation can be reduced by 5–7 mmag by removing a single mildly outlying point (1154R1, 0255R2, 0255R3 and 1539R1). This leaves only two data sets with $\sigma \geq 35$ mmag, namely 2036R1 and 1207R1, which can be described as genuinely noisy.

It is also noteworthy that for the confirmed variable 0746+2000 the largest standard deviation of 13 mmag was seen over nine runs in I; the minimum was only 7 mmag. A range of $5 \leq \sigma \leq 17$ mmag was measured for this object in the R band, over four runs.

6.2 Statistics in columns 10 and 11 of Table 2

Unfortunately, the p-value of the non-parametric function f_t is not useful as the sole indicator of variability: $p < 0.01$ for half of the UCD data sets, and for one-third of the comparison star data sets. This reflects the fact that the GAM procedure does not 'know' that small-scale trends in the data are caused by artefacts, and are not intrinsic to the star. The discriminatory power of the R^2 statistic may be greater: Fig. 15 (online only) compares its cumulative distribution functions for the UCD (solid line) and comparison star (broken line) data sets. Whereas only 11 per cent of the comparison data sets have e.g. $R^2 > 0.5$, the figure for the UCDs is 29 per cent. Corresponding figures for $R^2 > 0.6$ are 4 per cent (comparison stars) and 19 per cent (UCDs).

Of course, it is possible to have large values of R^2 even for non-variable objects, since the seeing-related part of the model may explain a substantial portion of the variability. The requirements $R^2 > 0.6$ and $p(\text{time}) < 0.01$ are met by only 3 per cent of the comparison star data sets, and 16 per cent of the UCD data, and this is what we adopt as the basic measure of intrinsic variability. The justification is subjective, resting on the visual examination of all the time-series data. In cases where model (3), rather than (2), has been fitted, the criteria are relaxed slightly to $p(\text{time}) < 0.01$ and $R^2 > 0.5$, since there is less model uncertainty.

In this way, 28 objects are taken to be variable. Four of these (0128−5545, 0428−2253, 0451−3402 and 1228−1547) are excluded because comparison stars show apparent variability of similar form and/or amplitude. The remaining 24 UCDs are listed as variable in Table 1.

Figs 16–34 (online only) show the estimated time dependence f_t for those data sets which satisfy the criteria for variability. For the 24 objects which are considered variable in at least one data set, criteria are relaxed to include also data sets with R^2 down to 0.5 [model (2)] or 0.4 [model (3)], but the requirement $p(\text{time}) < 0.01$ is retained in all cases. One qualifying data set is not plotted – 1159-52R4 – since it only consisted of 11 observations.

6.3 Comparison of the mean magnitudes from different observing runs

For those 68 objects with multiple runs in a given filter, the nightly mean magnitudes are compared in the last in the last column of Table 2. The values given are calculated with respect to the brightest mean value observed for a given UCD/filter, hence are all positive or zero. Since the zeros are not informative, the frequency distribution of only the strictly positive values is displayed in the top panel of Fig. 35. The corresponding information for the comparison star data is in the bottom panel of the figure: it should be borne in mind though that in some cases more than one of the comparison stars were used to determine the nightly zero-points, hence these data are not all independent.

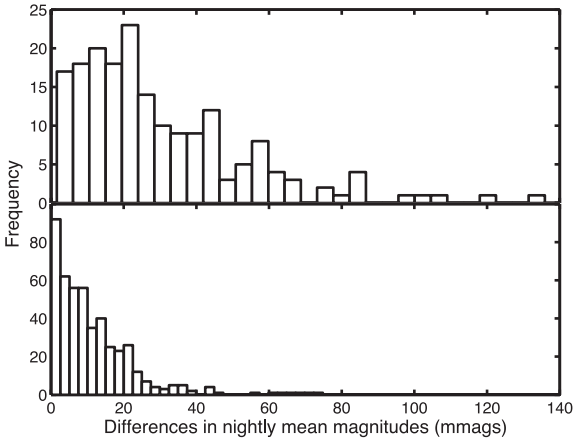

Figure 35. The distribution of mean magnitude levels where multiple time series were obtained for a given UCD/filter combination. Values shown are with respect to the brightest value of the collection, hence are all positive. Top panel: UCDs; bottom panel: comparison stars.

It is clear from the histograms that there is far less variability in the comparison star mean values: only 1.5 per cent of the 465 values exceed 50 mmag, whereas the corresponding number for the UCDs is 17 per cent. The appearance of the top histogram suggests an excess of values around 20 mmag, but the influence of seeing variations probably contributes substantially at this level. From a comparison of the two frequency distributions, a mean value difference of 50 mmag will be taken to be strong evidence for long-term (i.e. time-scales of days or longer) variability.

32 UCD mean value comparisons, shared amongst 19 objects, satisfy this criterion for variability. Four of these, for ϵ Indi Bab (0.136 mag), 1539−2952 (0.119 mag), 2130−0845 (0.105 mag) and 0559−1404 (0.102 mag), exceed one-tenth of a magnitude. It is noteworthy that neither 1539−2952 nor 0559−1404 shows evidence for short time-scale variability. A small minority (seven) of UCDs were observed multiple times in R, and only one of these (1159−5247) showed substantial changes in the mean brightness level.

Given that only about half the objects could be studied in this way, it may be speculated that the incidence of low-level long-term variability amongst UCDs may be quite high, at least in the I band.

7 PREVIOUS OBSERVATIONS

44 of the UCDs have been previously monitored for variability. This includes time-series runs in X-rays, optical, infrared, radio and spectroscopic monitoring. Both positive and null results are summarized below.

0036+1821. Following the detection of persistent radio emission, and also radio flares, by Berger (2002), an exhaustive multiwavelength study of this brown dwarf was performed by Berger et al. (2005). The authors find periodic radio emission ($P = 3.0$ h, i.e. 0.125 d) at 4.9 and 8.5 GHz, but no X-ray or Hα emission. The radio variability is far from sinusoidal, characterized primarily by

enhanced emission over 20 per cent of the cycle (0.025 d). The object was not detectable at longer wavelength Very Large Array observations (325 MHz; Jaeger et al. 2011).

Several hours of spectroscopic monitoring by Guenther et al. (2009) in the infrared did not reveal any variability. Gelino et al. (2002) found 0036+1821 non-variable in the *I* band. Maiti (2007) monitored the object in *R* and *I* over several nights; he/she observed distinct variability in *I* on one occasion (a dip in the light curve lasting ∼0.1 d), and what appears to be flaring behaviour in *R* on another night. Similar *I*-band variability was measured by Lane et al. (2007): a dip of several per cent, lasting of the order of 0.1 d. In the Lane et al. (2007) data set, this is preceded by a shallower depression in the light curve. The likely possibilities therefore appear to be a rapidly evolving periodicity of about 3 h, or a double wave light curve of double that period.

The present data showed variability in the two *I*-band runs (top panels of Fig. 16, in the online version of this paper) but not in *R*-band measurements contemporaneous with the second *I* run. The estimated time dependence suggests variability on time-scales of several hours. There is also a substantial (56 mmag) difference between the mean levels of the *I* data, obtained on successive nights. Further study of this object should be rewarding.

0058−0651. No photometric variability was detected in *I*-band monitoring by Gelino et al. (2002). A single new 2.6-h run in *I* did not show any brightness changes.

0144−0716. Substantial variability in Hα emission over the course of a few tens of minutes has been observed in this brown dwarf (Liebert et al. 2003); interestingly, emission was absent at a second epoch. The present data provide reasonable evidence for variability on two nights (Fig. 16, bottom panels, online only) and marginal evidence on the third. Judging by the different shapes of the two estimated functions f_t the brightness changes are aperiodic.

0205−1159. Monitoring in the NIR K_S band did not reveal any variability (Enoch, Brown & Burgasser 2003). One short (2 h) run in *I* (Table 2) likewise gave a null result.

0255−4700. About 8 h of monitoring by Clarke et al. (2008) ruled out variability in excess of 0.01 mag in the *J* band. This is in agreement with the earlier *JHK* photometric results of Koen et al. (2005), which found 0255−4700 to be constant. Morales-Calderón et al. (2006) and Morales-Calderón, Stauffer & Barrado y Navascués (2007) obtained mid-infrared time-series photometry, and concluded that 0255−4700 may possibly vary with a 7.4-h period at 4.5 μm, but that it appeared constant at 8 μm. Koen (2005) claimed variability on two different time-scales, ∼1.7 and ∼5 h, in his *I*-band observations. No variability was seen in a 3-h *R*-band run.

Seven data sets, in addition to the four described by Koen (2005), have been acquired. Three of these exhibit variability, according to the criteria of this paper (see Fig. 18, in the online version of this paper). There is little to suggest periodicity in the brightness changes. There is also variability on longer time-scales: the range of nightly means of the photometry is 69 mmag.

0320−0446. No overt signs of variability were found in JHK_S photometry obtained over several months by Blake et al. (2008). Two new *I*-band observing runs (Table 2) likewise gave null results. Both runs showed significant seeing dependence of the measured magnitudes, which may be due to the fact that the object is an unresolved double (see Table 1).

LP 412-31 (*0320+1854*). Substantial variability in Hα emission has been seen in this object (Schmidt et al. 2007). Stelzer et al. (2006) describe the detection of a large flare associated with LP 412-31, in both the *V* band and X-rays. However, a new 2.9-h run in *R* (Table 2) showed no flaring, or any other convincing signs of brightness changes.

0423−0414. Enoch et al. (2003) found the object to be possibly variable in the K_S band. Periodic variability (frequency 12 d^{-1}, amplitude 4 mmag) was observed by Clarke et al. (2008), from ∼8 h of monitoring in the *J* band. Koen et al. (2005) obtained a few *JHK* measurements spread over a three-week interval – these were consistent with the UCD being constant.

The noise level (σ = 19 mmag) of the data presented here is probably too high to allow the detection of variability at the level observed by Clarke et al. (2008).

0439−2953. There was no evident variability in 3.4 h of monitoring in *I* by Koen (2005). Re-analysis of those data confirms the result.

0445−3048. No variability was detected in three short *I*-band runs totalling 8 h (Koen 2004). Re-analysis of those data confirms that finding.

0451−3402. The *I*-band photometry collected by Koen (2004) (four runs, the longest being 4 h) could be phased together assuming an underlying 6.9-h periodicity. Re-analysis of the data suggests that the variability was more likely due to seeing changes. If the speculation by Koen (2009) is correct, this UCD would be a good target for multiplicity studies.

0523−1403. The object is a variable radio source (Antonova et al. 2007; see also Berger 2006; Osten et al. 2009; Berger et al. 2010). Koen (2005) did not see convincing evidence for *I*-band variability in two short photometric runs. Three further short observing runs on 0523−1403 (Table 2) did not reveal rapid variability either, but there is evidence for longer time-scale changes in that the range of the mean *I* magnitude over four runs was 63 mmag.

0539−0059. Bailer-Jones & Mundt (2001) measured 0539−0059 to be brighter by a few per cent on one of the four nights on which it was observed by them (in *I*). Spectral variability in the NIR was detected by Bailer-Jones (2008). The data of this paper (three *I*-band runs) provide marginal evidence for long time-scale variability (the range of nightly mean levels is 42 mmag), but there is no sign of rapid brightness changes.

0559−1404. Monitoring in the NIR K_S (Enoch et al. 2003) and *J* (Clarke et al. 2008) bands did not reveal any variability. Koen (2004) found a transient 16-min period in two of the six *I*-band photometric runs: it is conceivable that the origin was external to the UCD. Spectral variability in the NIR was observed by Bailer-Jones (2008).

Re-analysis of the Koen (2004) data did not reveal variability on time-scales of hours, but there are substantial changes in the mean brightness level from night to night, i.e. the object is variable on a time-scale of days.

0746+2000. Gelino et al. (2002) find a significant peak at 31 h in a periodogram of their *I*-band observations of this UCD, as well as possible variability on time-scales of tens of days. Maiti (2007) monitored the UCD in *R* and *I* and did not detect variability. Changes on a time-scale of about 3 h in the *I* magnitude of 0746+2000 were observed by Clarke, Oppenheimer & Tinney (2002b). No overt signs of variability were found in JHK_S photometry obtained over several months by Blake et al. (2008). Hα emission has been detected in 0746+2000 (Schmidt et al. 2007).

Two hours of observing at 4.9 GHz by Antonova et al. (2008) showed radio emission bursts. The most extensive variability study

of this binary UCD was carried out by Berger et al. (2009), who found periodic radio bursts at 4.9 GHz and a roughly sinusoidal modulation of Hα emission with the same period (2.1 h).

13 sets of observations of this UCD were acquired, eight of which satisfy the definition of short time-scale variability. It is noteworthy that none of the four *R*-band runs showed brightness changes. The estimated variations, plotted in Figs 20 and 21 (online only), show mostly non-monotonic behaviour. These figures strongly suggest that if there are periodicities in the optical data, then the time-scale should be longer than 4 h.

Nightly mean values of *I* span a range of 82 mmag.

0828−1309. Koen (2004) found clear evidence of *I*-band brightness changes in 0828−1309; a periodicity of 2.9 h (or its alias 3.3 h) fitted the data fairly well. A 3.1-h observing run in *R* by Koen (2005) did not show any variability. Spectral variability in the NIR was observed by Bailer-Jones (2008). Reiners & Basri (2008) determined that the Hα emission from the object is variable.

In addition to the observations by Koen (2004, 2005), another 11 runs on 0828−1309 were acquired: all of these were contemporaneous in the *R* and *I* bands. 10 of the total of 15 *I*-band time series had highly significant values of β_s; by contrast, seeing variations did not affect *R* magnitudes significantly. 12 of the data sets – one in *R*, the remainder in *I* – showed significant variability, according to the criteria of this paper. The estimated f_t are plotted in Figs 22–24 (online only). The estimated variability in *R*, in the upper right-hand panel of Fig. 24 (online only), appears compatible with the contemporaneous brightness changes in *I* in the adjacent panel of the figure. Variability is mostly aperiodic, although there are suggestions of cyclic brightness changes during some nights, particularly HJD 245 4127 and HJD 245 4148 (Fig. 23, online only). The successive brightness maxima on those two nights are separated by ∼1.5−1.6 d, i.e. 3.6–3.8 h.

The nightly mean *I* magnitudes span 58 mmag; the corresponding range in *R* is only 28 mmag.

0835−0819. The results of four *I*-band photometric runs were fitted by a 3.1-h period in Koen (2004). A 3.7-h observing run in *R*, on the other hand, did not show any variability (Koen 2005). Almost 10 h of monitoring did not find any radio emission at 4.8 GHz (Burgasser & Putman 2005).

Two of the five data sets acquired by Koen (2004) satisfy the variability criteria of this paper – the estimated functions f_t in equation (2) are plotted in the top two panels of Fig. 25 (online only). If there is an underlying periodicity, then the result for HJD 245 5358 suggests that it is slightly longer than 4 h.

0847−1532. A search for spectral variability in the NIR by Bailer-Jones (2008) gave a null result. Only one of the three *I*-band runs in the present study showed significant changes in brightness (Fig. 17, top right-hand panel, online only).

0909−0658. Time-series photometry in the *I* band obtained by Clarke et al. (2002b) did not reveal any variability. A null result also follows for the three observing runs logged in Table 2.

1045−0149. Monitoring for 3.5 h in the *I* band by Koen (2003) did not show any brightness changes. A second run of similar length (this paper) confirms that null result.

1048+0111. Time-series photometry in the *I* band obtained by Koen (2003) suggested possibly sinusoidal variability, but the data did not allow an unambiguous period to be determined. Reiners & Basri (2008) determined that the Hα emission from 1048+0111 is variable.

New data have been obtained (Table 2) and were analysed along with the observations reported by Koen (2003). Seven of the eight *I*-band time series, and two of the five *R*-band data sets, satisfy the definitions of variability; see Figs 26 and 27 (online only). The brightness changes are mostly aperiodic: if there is any underlying periodicity, it must be several hours.

1101−7718. This UCD is in the Cha I star-forming region. Spectral variability on a time-scale of hours indicates that it is probably an accretor (Scholz & Jayawardhana 2006). Evidence for outflows has also been observed (Muzzerolle et al. 2005). The object was constant for the duration of a single short (1.8 h) run in *I* (Table 2).

1139−3159. Almost 11 h of monitoring did not find any radio emission at 4.8 GHz (Burgasser & Putman 2005). There is some evidence for variability in the data presented here, but the runs are all too short to make definite statements ($T \leq 1.3$ h).

1159−5247. This UCD is a variable X-ray source (Hambaryan et al. 2004). 10 time series in the *I* and *R* bands were collected, but these are mostly quite short. Five data sets satisfy the definition of variability adopted in this paper; Fig. 28 (online only) shows the estimated f_t for four of these. (The duration of the fifth was only 1.2 h, with $N = 11$.) The estimated variability in *I* and *R* is rather different: this could be a real effect, or may simply reflect statistical uncertainty.

Mean nightly magnitudes varied considerably, ranges being 57 mmag for *I* and 76 mmag for *R*. The latter result is particularly noteworthy.

1228−1547. No photometric variability was detected in narrow-band monitoring by Tinney & Tolley (1999). There is some weak evidence for short time-scale variability in the longer of the two *I*-band runs on this UCD presented here. More impressively, the two nightly mean values differ by 68 mmag. Both runs show strong dependence of measured magnitudes on seeing: this may be caused by the fact that it is an unresolved double (see Table 1).

1300+1912. Observations by Gelino et al. (2002) in the *I* band showed a possible transitory long time-scale (9.9 d) periodicity. Aperiodic brightness changes in the *R* band were observed by Maiti et al. (2005) on a time-scale of hours. Littlefair et al. (2006) observed this UCD in g' and a narrow-band Na I filter: variability on a time-scale of several hours was seen, anticorrelated in the two filters.

Three short runs in *I*, and one in *R* (Table 2), did not provide evidence for rapid brightness changes.

1315−2649. Strong Hα emission from 1315−2649 is variable (Hall 2002a,b; see also the discussion and references in Burgasser et al. 2011). Monitoring in the *I* band for 2.9 h by Koen (2003) did not reveal any variability, and re-analysis of the data confirms the null result.

1409−3357. Weak evidence for variability in *I* was found by Koen (2003). Re-analysis suggests that this does not hold water, but two of the three further runs in *I* did show brightness changes of a few per cent (Table 2 and Fig. 29: see the online version of this paper). Note that a bright outlier has been excluded from the data from HJD 245 3185; the discrepant point has a substantial distorting influence on the model fitting for this particular set of observations.

1420−3613. Lee, Berger & Knapp (2010) measured changes in Hα emission on a time-scale of tens of minutes, but 1.3 h of *R*-band monitoring (this paper) did not show any variability.

1439+1929. Gelino et al. (2002) considered the object to be 'possibly variable' in the *I* band. Bailer-Jones & Mundt (2001) and

Bailer-Jones & Lamm (2003), respectively, monitored the UCD in *I* and JK' and found no brightness changes. Aperiodic brightness changes in the *R* band were observed by Maiti et al. (2005) on a time-scale of hours. Reiners & Basri (2008) determined that the Hα emission from 1439+1929 is variable.

The object was constant for the duration of one short run in *I* (Table 2).

1441−0945. Weak evidence for variability in *I* was found by Koen (2003). Littlefair et al. (2006) observed this UCD in g' and a narrow-band Na I filter, and saw no variability in about 3 h of monitoring. Re-analysis of the Koen (2003) data leads to the estimated f_t shown in Fig. 17, bottom left-hand panel (online only). A second run (see Table 2) did not show any variability.

1507−1627. No overt signs of variability were found in JHK_S photometry obtained over several months by Blake et al. (2008). Monitoring in the *I* band for 5 h by Koen (2003) did not reveal any variability, and re-analysis of those data confirms that 1507−1627 is constant.

1534−2952. Some slender evidence for short time-scale variability was seen by Koen et al. (2004) and Koen (2005); if present, variations are probably intermittent and aperiodic. Koen et al. (2005) obtained measurements on five nights over a period of 17 d, and found no systematic brightness changes. Time-series spectroscopy by Goldman et al. (2008) did not reveal any variability.

Re-analysis of the Koen (2004) optical data casts doubt on the presence of any brightness changes on time-scales of hours. The mean magnitude of the shortest run ($N = 7$) is 77 mmag fainter than the brightest of the four nightly means. Discounting this, the range of mean values is still 46 mmag, so that 1534−2952 does appear to vary on a time-scale of days.

1555−0956. 11 h of *I*-band monitoring by Koen (2005) did not give any convincing evidence of variability. Reiners & Basri (2008) determined that the Hα emission from 1555−0956 is variable. Re-analysis of the Koen (2005) data confirms his null result.

1636−0034. A little more than 3 h of *I*-band monitoring by Koen (2003) did not give any evidence of variability, a result confirmed by re-analysis of the data.

1645−1319. About 3 h of *I*-band monitoring by Koen (2003) showed the UCD to be constant. Re-analysis of the data confirmed the result.

1705−0516. About 23 h of monitoring in *I*, spread over six nights, led Koen (2005) to the identification of variability time-scales of ∼8.6 and ∼2.5 h. The estimated function f_t plotted in Fig. 30 (online only) suggests that the situation may not be so simple, and that brightness changes may be aperiodic. Note that (i) outliers have been excluded from the data sets obtained on HJD 245 3173 and HJD 245 3178, (ii) the influence of seeing on the measured magnitudes is highly significant in all but one of the seven data sets and (iii) the range of nightly mean magnitudes is quite large – 86 mmag.

2028+0052. There is no compelling evidence for variability in two *I*-band runs totalling 5.4 h (Koen 2003) or in 4.1 h of *JHK* monitoring (Koen et al. 2004). Re-analysis of the two optical photometric data sets leaves the previous conclusions unchanged.

2057−0252. Weak evidence for variability in *I* was found by Koen (2003). Littlefair et al. (2006) observed this UCD in g' and a narrow-band Na I filter, and saw no variability in about 5 h of monitoring. Re-analysis of the Koen (2003) observations confirms variability in the longer of the two data sets (Fig. 31, upper right-hand panel; online only).

2104−1037. Weak evidence for periodicities of ∼5 h (*I*) and ∼1.6 h (*JHK*) was presented by Koen (2005) and Koen et al. (2004), respectively. The NIR result could not be confirmed in two further short runs by Koen et al. (2005). The information in Table 2 suggests that the previously identified variability may have been due to seeing variations, rather than intrinsic to 2104−1037.

2130−0845. Slight evidence for variability was presented by Koen (2005), who identified a period of 1.5 h in three short *I*-band monitoring runs. No convincing signs of brightness changes were seen in NIR (*JHK*) photometry (Koen et al. 2004, 2005).

Variability in the data of Koen (2005) is not confirmed, but four further sets of measurements of 2130−0845 have been obtained (Table 2). Two of these satisfy the criteria of Section 6.2; the estimated brightness changes are plotted in the top two panels of Fig. 32 (online only). The mean levels of the two runs differed by a substantial 0.105 mag.

2158−1550. The 4.3-h *JHK* photometric run by Koen et al. (2004) did not reveal overt variability. A short new run in *I* (Table 2) also gave a null result.

ϵ *Indi Bab* (*2204−5646*). Mean *I*-band brightnesses of this brown dwarf measured 4 d apart differed by almost 0.1 mag, according to Koen (2003). Koen (2005) observed an almost perfectly linear brightness increase of more than 0.1 mag over the course of 3.6 h of *I*-band observing. Evidence for brightness differences of several per cent between NIR measurements taken ∼480 d apart was found by Koen et al. (2005). The 2.9-h *HK* photometric run obtained by Koen (2004) was too short to provide reliable information on flux changes.

Three new sets of observation of this T-dwarf binary have been acquired, in addition to the two runs by Koen (2003) and the one run by Koen (2005). All of these time series, including the one *R*-band data set, show strong dependence of the measured magnitudes on seeing. Four of the series exhibit short time-scale brightness changes (Fig. 33, online only). The shape of the estimated function f_t for the data acquired on HJD 245 3173 is far from the linear form fitted by Koen (2005), due to the inclusion of seeing as an independent variable. The level of true variability is also much smaller than suggested by the uncorrected light curve of the object.

There are considerable differences between the mean brightness levels of the different runs. The range spanned is 0.136 mag, the largest seen for any of the 125 target objects.

2224−0158. Gelino et al. (2002) found aperiodic variability in the *I* band. Four *I*-band runs by Koen (2005) totalling 15.7 h did not show any overt variability; neither did 2.3 h of *JHK* monitoring by Koen et al. (2004). Re-analysis of the Koen (2005) data confirms his null result.

8 NEW VARIABLES

There are 14 newly studied objects which are variable according to the criteria of this paper.

0228−6325. The variability estimated from a single 2.8-h run is plotted in Fig. 17 (top left-hand panel, in the online version of this paper). It would be interesting to see if further observations support the suggestion of a short time-scale periodicity.

Table 3. Objects with detailed individual descriptions in other papers by the author; in all cases, with the exception of the young brown dwarf 2MASS J1207334−393254a, the variability is either a clear-cut periodicity ('P'), large flares ('F') or both. Further observations are needed to verify whether the large amplitude variations in 2MASS J1207334−393254a are strictly periodic. For each object the number of observing runs, their total duration T and the total number of measurements obtained are given. The last column has a key to the references: 1 – Koen (2011); 2 – Koen (2005); 3 – Koen (2006); 4 – Koen (2003); 5 – Koen (2012); 6 – Koen (2008); 7 – Clarke et al. (2002a).

Name	Spectral type	No. of runs	T (h)	N	Var. type	Refs
DENIS-P J0041353−562112	M7.5	6	30.4	559	P+F	1
SSSPM J0109−5101	M8.5	5	32.5	759	P+F	2
2MASS 06050196−2342270	L0	3	11.4	231	P	3
2MASS J11553952−3727350	L2	9	55.9	1156	P	4,5
2MASS J1207334−393254a	M8	5	38.0	950	P?	6
Kelu-1	L2+L3.5	8	58.8	1473	P	7,5
DENIS-P J145407.8−640447	L3.5	8	41.9	1004	P	5

0641−4322. The mean *I*-band magnitudes of two runs, separated by three years, differed by 57 mmag.

0716−0630. Both sets of observations of 0716−2530 convincingly satisfy the variability criteria of this paper – see the top two panels of Fig. 19 (online only). The time-scale of brightness changes is evidently several hours.

0751−2530. The estimated variability functions of the object are plotted in the bottom two panels of Fig. 19 (online only). Note that the run on HJD 245 4553 was in the *R* band; a contemporaneous *I*-band data set did not show significant variability. The mean *I*-band brightness level of 0751−2530 also varied considerably (a range of 53 mmag).

0921−2104. Five of the eight time series of observations exhibited brightness variations (Fig. 34, online only).

1047−1815. The mean *I*-band magnitudes over four runs spanned 55 mmag.

1232−0951. The estimated time variation is plotted in the bottom two panels of Fig. 25 (online only). The result for HJD 245 4321, in particular, implies that the variability is either aperiodic or has a period of several hours.

1341−3052. The mean *I*-band magnitudes of two short runs, separated by 2 d, differ by 67 mmag.

1539−0520. There is strong evidence for changes in the mean *I*-band magnitude over time (range of 0.119 mag over five runs), but the mean magnitude in *R* seems constant (range of 21 mmag over three runs) or at least less variable.

1928−4356. The mean *I* magnitudes of two 4-h runs, separated by 1.3 yr, differ by 57 mmag.

2026−2943. One of the three *I*-band time series appears to be variable – see Table 2 and the top left-hand panel of Fig. 31 (online only).

2200−3038. A single set of measurements in *I* suggests variability (Fig. 31, bottom left; online only). The slope β_s in the fitted model (2) is highly significant.

2243−5932. Monitoring in white light for 3.7 h gave a time series which can be modelled by a linear brightness increase of about 0.04 mag (Fig. 31, bottom right; online only).

2351−2537. The two *I*-band runs (Table 2) both showed signs of variability – see the bottom two panels of Fig. 32 (online only).

9 CONCLUSIONS

(i) Of the 125 objects studied, 44 had been monitored for variability before. In about one-third of these objects, variability is confirmed; in another one-third, constancy is confirmed; and in the remainder of the cases, an opposite conclusion to the original is drawn from the present data.

(ii) Time-series studies of 81 objects are presented for the first time. Of these, seven vary only on time-scales of hours, five vary only on time-scales of days or longer and two show variability on both scales.

(iii) Categorization of the variability results in terms of spectral types is interesting. Out of 19 UCDs with variable mean magnitudes, only nine have spectral types earlier than L3. This contrasts with objects showing rapid variability – 18 out of 24 are of types L2 and earlier. Of the six so-called 'transition' objects with spectral types L8–T5 (e.g. Goldman 2005; Radigan et al. 2012), four show long-term brightness changes.

(iv) When considering the numbers in (iii) it is also useful to bear in mind the number of targets of the various spectral types. All three T dwarfs in the study showed changes in nightly mean levels; in one of these there was also evidence for variability on time-scales of hours. Data for only two out of 16 M dwarfs satisfied the criteria for short time-scale variability, and one of these was also variable on longer time-scales. The long time-scale brightness changes of two of the three T dwarfs are amongst the largest measured in the entire sample, exceeding one-tenth of a magnitude (Section 6.3). Mean magnitude changes in the single M dwarf showing this phenomenon were also substantial – up to 57 and 76 mmag in *I* and *R*, respectively.

(v) In order to draw more general conclusions, additional information from other studies by the author is summarized in Table 3. Variability in the objects listed there is of a nature (periodic and/or large flares) which does not require statistical methods for extraction. Combining the information from this paper and Table 3, 19 M dwarfs, 109 L dwarfs and three T dwarfs were observed for a total of, respectively, 160, 968 and 60 h. Sustained flares were only observed in two M dwarfs, giving a flaring incidence amongst these objects of about 11 per cent. Rough upper limits of 0.001 and 0.017 flares h^{-1} can be deduced for the L and T dwarfs, respectively, at least at a level exceeding a few per cent in the *I* band. Persistent periodic variability was seen in only three M dwarfs and four L dwarfs; the latest spectral type of any periodic variable is L3.5. Note though that periodicities longer than several hours would not have been uncovered by the relatively short observing runs. It is noteworthy

that there are also changes in the mean brightness levels of all three periodic L dwarfs, whereas amongst the M-type objects in Table 3 only the very young brown dwarf 2MASS J1207334−393254a exhibits this phenomenon. (It is also the only UCD in Table 3 which shows rapid aperiodic variability.)

Including the information in Table 3, the percentages of objects showing variability on time-scales of days are 11, 17 and 100 per cent for M, L and T spectral types, respectively. Variability on time-scales of hours (both periodic and aperiodic) is seen in 26, 23 and 33 per cent of the M, L and T dwarfs (but note that the last figure is based on variability in a single object).

(vi) To the author's mind the most important conclusion to be drawn from this study is that clear-cut rapid (time-scale 1–3 h), sustained *I*-band variability with amplitudes exceeding 10 mmag or so, is rare in UCDs. When variability does occur it mostly seems to be aperiodic and intermittent.

(vii) It is also clear that optical flares of any substance are very rare, if not completely absent, in L and T dwarfs, at least in *I* (and probably *R*).

(viii) Secure identification of variability from data such as those presented in this paper remains a problem. A related issue is the modelling of the influence of seeing on the measured magnitudes. It seems likely that there is some confounding of time and seeing effects, but is not obvious what – if anything – can be done to reliably unravel the two. If multiplicity is indeed an underlying cause of the dependence of magnitude on seeing, then those objects for which the effect is more evident would be good targets for high-resolution visual, or interferometric studies.

(ix) For reasons such as mentioned in (viii), data sets are made available, so that interested readers can perform their own analyses and draw their own conclusions.

ACKNOWLEDGMENTS

The author thanks the South African Astronomical Observatory for allocating the telescope time necessary to complete the time-consuming project, and the technical staff at Sutherland for maintaining the equipment. He is also very grateful to those running the SIMBAD data base in Strasbourg, France, and to those who contributed to producing the DENIS, 2MASS and SDSS catalogues. This paper was completed while visiting the Experimental Astrophysics Group of the Space Sciences Laboratory (University of California, Berkeley). The author is grateful to that institution, and to Prof. Oswald Siegmund and Dr Barry Welsh in particular, for the hospitality.

REFERENCES

Adelman-McCarthy J. K. et al., 2009, ApJS, 182, 543
Antonova A., Doyle J. G., Hallinan G., Golden A., Koen C., 2007, A&A, 472, 257
Antonova A., Doyle J. G., Hallinan G., Bourke S., Golden A., 2008, A&A, 487, 317
Artigau E., Nadeau D., Doyon R., 2003, in Martín E. L., ed., Proc. IAU Symp. 211, Brown Dwarfs. Astron. Soc. Pac., San Francisco, p. 451
Artigau E., Bouchard S., Doyon R., Lafrenière D., 2009, ApJ, 701, 1534
Bailer-Jones C. A. L., 2008, MNRAS, 384, 1145
Bailer-Jones C. A. L., Lamm M., 2003, MNRAS, 339, 477
Bailer-Jones C. A. L., Mundt R., 2001, A&A, 367, 218
Berger E., 2002, ApJ, 572, 503
Berger E., 2006, ApJ, 648, 629
Berger E. et al., 2005, ApJ, 627, 960
Berger E. et al., 2009, ApJ, 695, 310
Berger E. et al., 2010, ApJ, 709, 332
Bernat D. et al., 2010, ApJ, 715, 724
Blake C. H., Bloom J. S., Latham D. W., Szentgyorgyi A. H., Skrutskie M. F., Falco E. E., Starr D. S., 2008, PASP, 120, 860
Blake C. H., Charbonneau D., White R. J., 2010, ApJ, 723, 684
Bouy H. et al., 2003, AJ, 126, 1526
Burgasser A. J., McElwain M. W., 2006, AJ, 131, 1007
Burgasser A. J., Putman M. E., 2005, ApJ, 626, 486
Burgasser A. J., Liebert J., Kirkpatrick J. D., Gizis J. E., 2002, AJ, 123, 2744
Burgasser A. J., Kirkpatrick J. D., Reid I. N., Brown M. E., Miskey C. L., Gizis J. E., 2003, ApJ, 586, 512
Burgasser A. J., Reid I. N., Leggett S. K., Kirkpatrick J. D., Liebert J., Burrows A., 2005, ApJ, 634, L177
Burgasser A. J., Cruz K. L., Kirkpatrick J. D., 2007a, ApJ, 657, 494
Burgasser A. J., Looper D. L., Kirkpatrick J. D., Liu M. C., 2007b, ApJ, 658, 557
Burgasser A. J. et al., 2010, ApJ, 710, 1142
Burgasser A. J., Sitarski B. N., Gelino C. R., Logsdon S. E., Perrin M. D., 2011, ApJ, 739, 49
Caballero J. A., Béjar V. J. S., Rebolo R., 2003, in Martín E. L., ed., Proc. IAU Symp. 211, Brown Dwarfs. Astron. Soc. Pac., San Francisco, p. 455
Clarke F. J., Tinney C. G., Covey K. R., 2002a, MNRAS, 332, 361
Clarke F. J., Oppenheimer B. R., Tinney C. G., 2002b, MNRAS, 335, 1158
Clarke F. J., Tinney C. G., Hodgkin S. T., 2003, MNRAS, 341, 239
Clarke F. J., Hodgkin S. T., Oppenheimer B. R., Robertson J., Haubois X., 2008, MNRAS, 386, 2009
Close L. M., Siegler N., Freed M., Biller B., 2003, ApJ, 587, 407
Cody A. M., 2007, in Stancliffe R. J., Dewi J., Houdek G., Martin R. G., Tout C. A., eds, AIP Conf. Proc. Vol. 948, Unsolved Problems in Stellar Physics. Am. Inst. Phys., New York, p. 125
Dahn C. C. et al., 2002, AJ, 124, 1170
Dahn C. C. et al., 2008, ApJ, 686, 548
Enoch M. L., Brown M. E., Burgasser A. J., 2003, AJ, 126, 1006
Epchtein N. et al., 1999, A&A, 349, 236 (DENIS catalogue)
Gelino C. R., Burgasser A. J., 2010, AJ, 140, 110
Gelino C. R., Marley M. S., Holtzman J. A., Ackerman A. S., Lodders K., 2002, ApJ, 577, 433
Goldman B., 2005, Astron. Nachr., 326, 1059
Goldman B. et al., 2008, A&A, 487, 277
Guenther E. W., Zapatero Osorio M. R., Mehner A., Martín E. L., 2009, A&A, 498, 281
Hall P. B., 2002a, ApJ, 564, L89
Hall P. B., 2002b, ApJ, 580, L77
Hambaryan V., Staude A., Schwope A. D., Scholz R.-D., Kimeswenger S., Neuhäuser R., 2004, A&A, 415, 265
Hastie T. J., Tibshirani R. J., 1990, Generalized Additive Models. Chapman & Hall, London
Jaeger T. R., Osten R. A., Lazio T. J., Kassim N., Mutel R. L., 2011, AJ, 142, 189
Jao W.-C., Mason B. D., Hartkopf W. I., Henry T. J., Ramos S. N., 2009, AJ, 137, 3800
Kendall T. R., Jones H. R. A., Pinfield D. J., Pokorny R. S., Folkes S., Weights D., Jenkins J. S., Mauron N., 2007, MNRAS, 374, 445
Koen C., 2003, MNRAS, 346, 473
Koen C., 2004, MNRAS, 354, 378
Koen C., 2005, MNRAS, 360, 1132
Koen C., 2006, MNRAS, 367, 1735
Koen C., 2008, MNRAS, 389, 949
Koen C., 2009, MNRAS, 395, 531
Koen C., 2011, MNRAS, 411, 1197
Koen C., 2012, submitted
Koen C., Matsunaga N., Menzies J., 2004, MNRAS, 354, 466
Koen C., Tanabé T., Tamura M., Kusakabe N., 2005, MNRAS, 362, 727
Koen C., Kanbur S., Ngeow C., 2007, MNRAS, 380, 1440
Kovács G., Bakos G., Noyes R. W., 2005, MNRAS, 356, 557
Lane C. et al., 2007, ApJ, 668, L163
Lee K.-G., Berger E., Knapp G. R., 2010, ApJ, 708, 1482

Liebert J., Gizis J. E., 2006, PASP, 118, 659
Liebert J., Kirkpatrick J. D., Cruz K. L., Reid I. N., Burgasser A., Tinney C. G., Gizis J. E., 2003, AJ, 125, 343
Littlefair S. P., Dhillon V. S., Marsh T. R., Shahbaz T., Martín E. L., 2006, MNRAS, 370, 1208
Luhman K. L., 2007, ApJS, 173, 104
Maiti M., 2007, AJ, 133, 1633
Maiti M., Sengupta S., Parihar P. S., Anupama G. C., 2005, ApJ, 619, L183
Martín E. L., Zapatero Osorio M. R., Lehto H. J., 2001, ApJ, 557, 822
McCaughrean M. J., Close L. M., Scholz R.-D., Lenzen R., Biller B., Brandner W., Hartung M., Lodieu N., 2004, A&A, 413, 1029
Meyer F., Meyer-Hofmeister E., 1999, A&A, 341, L23
Morales-Calderón M. et al., 2006, ApJ, 653, 1454
Morales-Calderón M., Stauffer J. R., Barrado y Navascués D., 2007, Rev. Mex. Astron. Astrofis., 29, 40
Muzzerolle J., Luhman K. L., Briceño C., Hartmann L., Calvet N., 2005, ApJ, 625, 906
Osten R. A., Phan-Bao N., Hawley S. L., Reid I. N., Ojha R., 2009, ApJ, 700, 1750
Palla F., Baraffe I., 2005, A&A, 432, L57
Phan-Bao N. et al., 2008, MNRAS, 383, 831
Radigan J., Jayawardhana R., Lafrenière D., Artigau É., Marley M., Saumon D., 2012, ApJ, 750, 105
Reid I. N., Lewitus E., Burgasser A. J., Cruz K. L., 2006a, ApJ, 639, 1114
Reid I. N., Lewitus E., Allen P. R., Cruz K. L., Burgasser A. J., 2006b, AJ, 132, 891
Reid I. N., Cruz K. L., Burgasser A. J., Liu M. C., 2008, ApJ, 135, 580
Reiners A., 2012, Living Rev. Sol. Phys., 8, 1
Reiners A., Basri G., 2008, ApJ, 684, 1390
Rockenfeller B., Bailer-Jones C. A. L., Mundt R., Ibrahimov M. A., 2006, MNRAS, 367, 407
Schechter P. L., Mateo M., Saha A., 1993, PASP, 105, 1342
Schmidt S. J., Cruz K. L., Bongiorno B. J., Liebert J., Reid I. N., 2007, AJ, 133, 2258
Scholz A., Jayawardhana R., 2006, ApJ, 638, 1056
Skrutskie M. F. et al., 2006, AJ, 131, 1163 (2MASS catalogue)
Stelzer B., Schmitt J. H. M. M., Micela G., Liefke C., 2006, A&A, 460, L35
Tinney C. G., Tolley A. J., 1999, MNRAS, 304, 119
Wood S., 2006, Generalized Additive Models: An Introduction with r. Chapman & Hall/CRC, Boca Raton, Florida

SUPPORTING INFORMATION

Additional Supporting Information may be found in the online version of this article:

Table 2. The observing log (columns 2–6), and some quantities derived from the photometry (columns 7–12).

Figures 11 and 14–34.
Zip file. A file (data.zip) containing 353 datasets (http://mnras.oxfordjournals.org/lookup/suppl/doi:10.1093/mnras/sts208/-/DC1).

Please note: Oxford University Press are not responsible for the content or functionality of any supporting materials supplied by the authors. Any queries (other than missing material) should be directed to the corresponding author for the article.

This paper has been typeset from a TEX/LATEX file prepared by the author.